UNIVERSITY OF HELSINKI REPORT SERIES IN PHYSICS

HU-P-D89

Non-Rutherford Elastic Scattering Cross Sections for Materials Analysis

Arto Nurmela

Accelerator Laboratory
Department of Physics
Faculty of Science
University of Helsinki
Helsinki, Finland

ACADEMIC DISSERTATION

To be presented, with the permission of the Faculty of Science of the University of Helsinki, for public criticism in Auditorium XII of the main building of the University, on April 18th, 2001, at 10 o'clock a.m.

HELSINKI 2001

ISBN 951-45-9894-6 (PDF version)

Helsinki 2001

Helsingin yliopiston verkkojulkaisut

A. Nurmela: **Non-Rutherford elastic scattering cross sections**, University of Helsinki, 2001, 34 p.+appendices, ISBN 951-45-9894-6 (PDF version)

Keywords (INSPEC): non-Rutherford, elastic scattering, cross section

ABSTRACT

In this thesis the non-Rutherford elastic scattering cross sections of hydrogen, helium, lithium and boron ions for several target elements have been investigated. To broaden the useable ion energy region for materials analysis methods, e.g., backscattering and elastic recoil detection analysis, from pure Rutherford scattering region to scattering in which the nuclear effects arise, the non-Rutherford elastic scattering cross section have been experimentally determined.

Proton scattering by helium, natural copper, molybdenum, silver and tin have been measured at ion energies below 7 MeV through several scattering angles. Helium, lithium and boron ion scattering by natural nickel have been measured near the Coulomb barrier. The backscattering angles were selected so that by kinematically reversing the reaction, the recoil angles are 20°, 30° and 40°. The scattering cross sections or ratios of the cross section to Rutherford cross section have been given in the non-Rutherford energy region.

The threshold energies for the non-Rutherford energy, above which the scattering of the ion is not purely from the Coulomb potential of the target atom and the cross section starts to deviate 4% or more from its Rutherford value, have been given. Also a model to predict the threshold energy for non-Rutherford cross section at large scattering angles is presented.

Optical model calculations were used to determine the elastic scattering cross sections, the shape and dimensions of the target atom potential. With the optical model calculations the elastic scattering cross sections were determined at non-measured energies and scattering angles and interpolated between the measured data points.

CONTENTS

ABSTRACT **1**

1 INTRODUCTION **4**

2 STRUCTURE AND PURPOSE OF THIS STUDY **6**

3 ELASTIC COLLISIONS **8**

3.1 Kinematics of the elastic collision 9

3.2 Elastic scattering cross sections 12

3.2.1 Rutherford cross sections 12

3.2.2 Non-Rutherford cross sections 12

3.2.3 Shape-elastic scattering 13

3.2.4 Compound elastic scattering 14

3.2.5 Resonances and resonance scattering 15

3.2.6 Threshold energy for non-Rutherford cross sections 15

4 EXPERIMENTAL METHODS **17**

4.1 Determination of the scattering cross sections 18

4.2 The optical model in scattering analysis 22

5 SUMMARY OF RESULTS **23**

5.1 Proton scattering 23

5.2 Helium ion scattering 25

5.3 Lithium and boron ions 25

5.4 Model for the non-Rutherford threshold energy 25

6 CONCLUSIONS **29**

ACKNOWLEDGEMENTS **31**

REFERENCES **32**

1 INTRODUCTION

The era of ion beam experiments in nuclear physics started with Geiger's and Marsden's experiments with alpha particles from an alpha source and a very thin gold leaf target [1]. They bombarded the golden leaf with MeV energy alpha particles and studied the angular distribution of ions scattered in collision with the target. These experiments proved the theory developed by Ernest Rutherford of the Coulomb scattering model of the scattering cross sections [2].

Rutherford's scattering event is based on the electrical interaction between the ion and the target. It is now quite simple to derive the theoretical formulation for the scattering cross section of this event. The Rutherford cross sections have been used in the appropriate energy and particle mass regions in nuclear physics and materials science for many decades.

Modern ion beam analysis was initiated in the fifties. By using proton backscattering Rubin and Rasmussen studied smog [3] and Sippel measured the diffusion of Au into Cu [4]. Maybe the most famous alpha-scattering experiment was to analyze the composition of the lunar soil [5]. This experiment was the first widely published practical application of the ideas of Rutherford, Geiger and Marsden to a problem of nonnuclear interest.

Quantitative analyses with ion beam analysis (IBA) techniques are based on the knowledge of the interaction cross sections. In materials science with ion beams the elemental, quantitative and depth distribution analyses of the studied sample are the main goals. The most important analytical method is the ion backscattering technique [6]. Conventionally, the method is called Rutherford backscattering spectrometry (RBS) and the analysis is done in the energy, angle and particle mass region where the scattering is assumed to take place from the Coulomb potential.

Rutherford backscattering spectrometry is an established analytical technique, with the characteristics of the technique well known. The surface and shallow depths of solid samples can be analyzed for elemental depth distributions with good sensitivity for high mass elements and good mass separation

for low mass elements. The weaknesses are related to the opposite conditions; sensitivity of detecting light elements and low mass separation of heavy elements.

In recent years, arising from ever-increasing needs of materials physics applications, RBS has been developed to overcome its inherent weaknesses. Higher ion energies lead to larger probing depths, better mass resolution for heavy elements and often higher detection sensitivities for light elements. As a consequence, the simple Rutherford model has to be abandoned since the nuclear effects begin to contribute. With the higher energies, the cross sections may vary even by magnitudes from Rutherford and the exact values can not be predicted theoretically. Therefore, experimental scattering cross section data for the higher ion energies are needed.

Experimentally one can also determine the threshold energy for the non-Rutherford scattering from the experimental scattering cross section excitation curve. With the knowledge of the threshold energy the ion energy may be limited so that the scattering is purely Rutherford when, for example, the cross sections become too small above the threshold.

Another analytical technique based on the same elastic collision is called the elastic recoil detection analysis (ERDA). In ERDA the heavier ion collides with the lighter target atom which recoils after the collision. The recoiled target atom is then detected.

ERDA is nowadays used in elemental analysis and depth profiling as a standard procedure. As with backscattering, the knowledge of the cross sections is necessary for quantitative analysis with the ERDA technique. Cross sections exceeding the Coulomb cross sections lead to enhanced detection sensitivities. The ion energy threshold for the non-Rutherford scattering in elastic recoil detection analysis is much higher than in backscattering spectrometry because of the kinematics. With appropriate ion-target pairs the threshold still may be reached and unwanted nuclear effects may arise.

Optical model (OM) is a powerful tool to calculate the cross sections over a wide range of ions, ion beam energies and scattering angles [7] and it has been used as a basic tool in nuclear physics for

many decades. In the OM calculations, the theoretical scattering model is under study and the ions are treated as plane waves in these calculations. The plane waves scatter by the spherical target atom in the collision and after the collision the scattered waves are treated as spherical waves. The shape and dimensions of the target atom's potential may be characterized with the wave number and the wave length before and after the collision.

As the analytical techniques RBS and ERDA are two faces of the same elastic collision, the same kinematical treatment applies to them both. In this thesis the kinematical reversal has been applied to convert the ion energy, the scattering angle and elastic scattering cross sections from backscattering spectrometry to elastic recoil detection analysis.

2 STRUCTURE AND PURPOSE OF THIS STUDY

This thesis consists of the summary and the following six articles which are referred to by Roman numbers. A brief summary of the articles included is given below.

Article I: Elastic scattering cross sections of protons by copper, molybdenum, silver and tin near the Coulomb barrier, A. Nurmela, V. Zazubovich, J. Räisänen, E. Rauhala and R. Lappalainen *Journal of Applied Physics* **84**, (4) (1998) 1796-1799.

> The elastic scattering cross sections of protons by copper, molybdenum, silver and tin are determined experimentally at energies below 6.5 MeV through scattering angles of 135° and 165°. Part of the focus is in the threshold energy where the Rutherford cross section becomes invalid. A brief literature survey of the proton elastic scattering cross sections by lighter elements is included in the article.

Article II: Elastic scattering cross sections for the *p*+He system in the energy region of 1.4 - 24 MeV, A. Nurmela E. Rauhala and J. Räisänen, *Journal of Applied Physics* **82** (5) (1997) 1983-1988.

> Proton backscattering by helium and helium recoil scattering by hydrogen have been investigated. Wide proton and helium ion energy ranges and large distribution of scattering angles, which are typical in materials analysis, have been studied.

Article III: Elastic scattering cross sections for the analysis of helium by ^{1}H backscattering and hydrogen by ^{4}He ERD, A. Nurmela E. Rauhala and J. Räisänen, *Nuclear Instruments and Methods*

in Physics Research **B 136-138** (1998) 77-80.

The ratio of the cross section to Rutherford cross section for proton backscattering by helium through scattering angles of 110° to 160° has been investigated. Data for the kinematically reversed elastic recoil scattering are presented.

Article IV: Elastic scattering cross sections for ^{6}Li and ^{7}Li scattering by aluminum, silicon and titanium below 12 MeV at angles of 140° and 170°, A. Nurmela E. Rauhala and J. Räisänen, *Nuclear Instruments and Methods in Physics Research* **B 155** (1999) 211-220.

The contribution of the isotopic effect to the scattering cross sections and in the threshold energy has been studied. Most of the threshold energy models are more or less linearly dependent on ion and target mass so that the heavier mass predicts higher threshold energy. In this article is shown that a lighter isotope of the ion may have higher threshold energy than heavier isotope in the scattering by the same target element through the same scattering angle.

Article V: RBS and ERD cross sections and optical model parameters for the analysis of lithium, boron and nickel, A. Nurmela, P. Pusa, E. Rauhala and J. Räisänen, *Nuclear Instruments and Methods in Physics Research* **B 161- 163** (2000) 130-135.

The article deals with optical modeling of the elastic scattering excitation curve as a function of energy and scattering angle. Results of the scattering model have been compared with experimentally determined elastic scattering cross sections.

Article VI: He + Ni elastic scattering near the Coulomb barrier and optical model parameters, A. Nurmela, P. Pusa, E. Rauhala and J. Räisänen, *Journal of Applied Physics*, submitted for publication.

The energy and angular distribution of scattering cross sections for helium ion scattering by nickel have been measured. The developed optical model code has been applied to new experimental elastic scattering cross section data.

Publications are result of group work. All measurements and experimental data analysis were done by the author except in article **I** in which some of the measurements and data analyses were done by a co-author. The author was the responsible author in all of the articles writing most of the articles **I**, **IV** - **VI** and participated in writing articles **II** and **III**.

The purpose of the thesis is to present new non-Rutherford scattering cross section data for backscattering and recoil scattering systems. The new cross section data provide a data base for theoretical

calculations in nuclear physics and optical model (OM) calculations. With accurate cross sections the nuclear model may be further elaborated. For example, the resonances in the cross sections reflect the excitation states of the nucleus. With the OM we get more accurate forms of the nuclear potentials. Also, with the OM the cross sections may be extrapolated into the non-measured energies and angles.

In the case where the Rutherford cross sections are not valid due to nuclear effects the accurate cross sections have to be known in IBA based applications. Depending on the masses of the ion and the target the cross sections may increase or fall off. The new cross section data extends RBS and ERDA applicability to broader energy range and wider scattering angle distribution. In the thesis the safe energy limits for the Coulombic scattering have been investigated as well. There are several threshold energy models and in the thesis a more accurate threshold energy model is given.

A thin film areal density hydrogen standard in many research and development areas in industrial applications is of great importance. The thin film areal density hydrogen standard is a sample in which the hydrogen content is known very accurately. The sample may be taken as a reference when other samples with hydrogen content are studied. In semiconductor technology, for example, the hydrogen standard is needed because of dielectric properties of hydrogen in semiconductors. As a common impurity on the sample surfaces, hydrogen always plays some role in ion beam analysis. By bombarding helium ions into the thin film target the surface density of hydrogen atoms may be determined by ERDA. The cross sections for the $^{1}H(^{4}He,p)^{4}He$ reaction are thus important in the hydrogen detecting process. A collaboration to prepare a hydrogen standard is briefly described in Section 6.

3 ELASTIC COLLISIONS

According to the scattered particles the ion-target collisions may be divided into four distinct events: Elastic scattering by electrons of the target atom, inelastic scattering by the electrons of the target atom, elastic scattering by the nucleus of the target atom and inelastic scattering by the nucleus of the

target atom. Basic phenomena studied in this thesis are the ion elastic scattering by the nucleus of the target atom and scattering near the Coulomb barrier of the target atom and by its nuclear potential.

3.1 Kinematics of the elastic collision

In the scattering process the accelerated ion collides with and scatters by the target. After the collision through a certain scattering angle the scattered ions are detected. The scattering angle may vary from 0° to 180°. In applications the mass of the ion is usually smaller than the mass of the target atom. In the elastic recoil process the ions give recoil energy to the target atoms and after the collision the recoiled atoms are detected. The recoiled atoms scatter through recoil angles less than 90°. When this process is used as an analytical tool, the ion is typically heavier than the target.

The kinematics of elastic backscattering is described in terms of the kinematic factor K. The K value is defined as energy of the scattered ion divided by the initial ion energy. Fig. 1 shows the K values for protons, ^{4}He, ^{7}Li, ^{11}B and ^{12}C ions as a function of target mass through scattering angle of 170°.

The kinematic factor K follows from the conservation of the momentum and energy. With the K value the energy of the elastically scattered ions may be determined and separated from the inelastically scattered ions. The knowledge of the energy of the scattered ion is important in the measurements when several peaks are observed in the spectrum. This is due to the yield from different elements and their isotopes and also from the reaction products in the scattering event. The elastic peak of the element may be determined by multiplying the initial ion energy with the K value. Also, if the nuclear reactions occur the energies of separate reaction products may be calculated.

The ion-target system in backscattering process may be converted to the recoil process by kinematically reversing the reaction. This can be done by first changing the coordinates from the laboratory to the center of mass frame of reference. In the center-of-mass system the initial ion or target are not distinguishable. By exchanging the roles of the initial ion and target and by converting back to

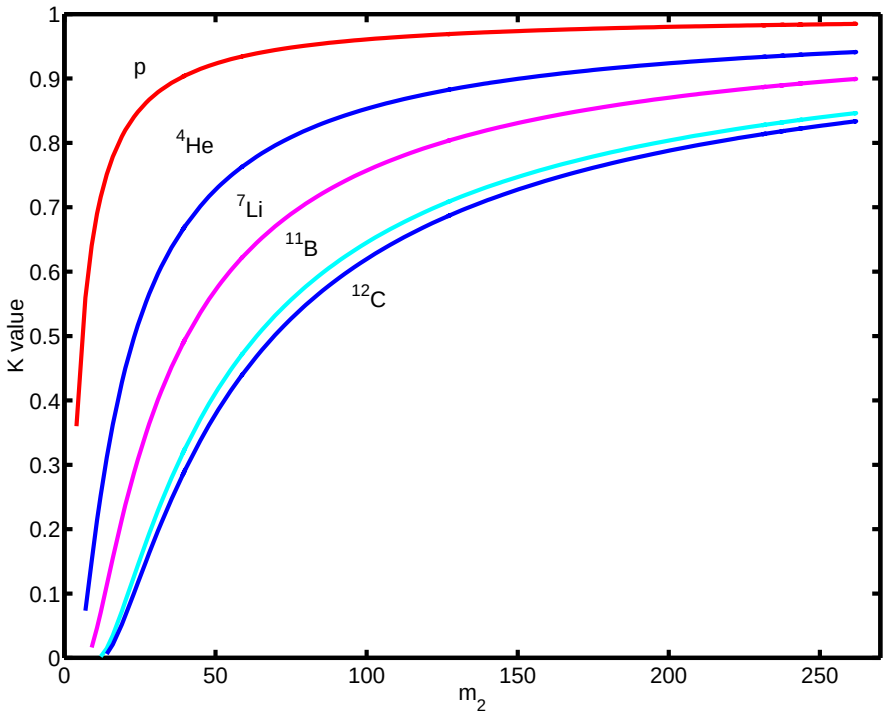

Figure 1: The kinematic factor K values for protons, ^{4}He, ^{7}Li, ^{11}B and ^{12}C ions as a function of target mass through the scattering angle of 170°.

the laboratory frame of reference, the quantities describing the kinematics of a reversed process are achieved.

The converted ion energy from the laboratory coordinates to center of mass frame is $E_{cm} = E_{lab}(1 + m_1/m_2)$, where m_1 and m_2 are the masses of the incident ion and target, respectively. From this we get a ratio between ion energies in elastic recoil detection (ERD) and in backscattering spectrometry (BS), $E_{ion,ERD} = E_{ion,BS} m_{target,BS}/m_{ion,BS}$, where $E_{ion,ERD}$ is the energy of the ion in ERD, $E_{ion,BS}$, $m_{target,BS}$ and $m_{ion,B}$ are the energy of the ion in BS, the mass of the target atom in BS and the mass of the ion in BS. The relation between the backscattering angle θ in the laboratory coordinates and in the center of mass frame is

$$\theta_{cm} = \arcsin\left(\frac{m_{ion}}{m_{target}} \sin\theta\right) + \theta. \quad (1)$$

The recoil angle in the center of mass frame of reference is $\varphi_{cm} = \pi - \theta_{cm}$. The relation between the recoil angle φ in the laboratory and center of mass frames of reference is $\varphi = \varphi_{cm}/2$. The formulas above give the energy and angular conversions from backscattering to recoil geometry.

A conversion for the cross sections from backscattering to elastic recoil scattering is obtained as follows. The backscattering cross section ratio between the laboratory and the center of mass frame is

$$\frac{d\sigma_{lab}^{BS}(\theta)}{d\sigma_{cm}^{BS}(\theta_{cm})} = \frac{\sin^2\theta_{cm}}{\sin^2\theta_{lab}} \frac{1}{\cos(\theta_{cm} - \theta_{lab})} \tag{2}$$

and the corresponding ratio for recoil cross section is obtained by the equation

$$\frac{d\sigma_{lab}^{ERD}(\varphi)}{d\sigma_{cm}^{ERD}(\varphi_{cm})} = 4\cos\varphi. \tag{3}$$

According to principle of detailed balance [8] the scattering cross section is equal to recoil cross section in the center of mass frame of reference. By taking this into account and combining Equations (2) and (3) we get the expression for the ratio between the recoil and backscattering cross section in the laboratory frame as

$$\frac{d\sigma_{lab}^{ERD}}{d\sigma_{lab}^{BS}} = 4\cos\varphi\cos(\theta_{cm} - \theta_{lab}) \frac{\sin^2\theta_{lab}}{\sin^2\theta_{cm}}. \tag{4}$$

The recoil cross sections are obtained this way by scaling from the direct cross section values for each angle and energy. The ratios of cross sections to Rutherford cross sections $d\sigma/d\sigma_{Ruth.}$ are equal for the direct and recoil scattering processes with converted energies to recoil or backscattering events.

3.2 Elastic scattering cross sections

3.2.1 Rutherford cross sections

Rutherford cross section in the laboratory frame of reference is

$$\frac{d\sigma}{d\Omega} = \left(\frac{Z_1 Z_2 e^2}{16\pi\varepsilon_0 E}\right)^2 \frac{4}{\sin^4\theta} \frac{\left[\sqrt{1-\left(\frac{m_1}{m_2}\right)^2 \sin^2\theta} + \cos\theta\right]^2}{\sqrt{1-\left(\frac{m_1}{m_2}\right)^2 \sin^2\theta}}, \tag{5}$$

where Z_1 and Z_2 are atomic numbers and m_1 and m_2 are the masses of ion and target, respectively. E is the incident laboratory energy of the ion and θ is the laboratory scattering angle. The Rutherford cross sections describe the interaction probability in the Coulombic collisions between the ion and the target. In the thesis the experimental cross section values are compared with Rutherford cross sections.

3.2.2 Non-Rutherford cross sections

Non-Rutherford elastic scattering cross sections appear when the ion energy is so high that the ion starts penetrate the Coulomb barrier of the target atom. When the ion penetrates the Coulomb barrier of the target atom, the scattering is from the target atom's nuclear potential and the effect of the nuclear forces for the scattering then become significant. Also resonances may cause significant deviation to the scattering cross section from its Rutherford value.

When the ion energy is low enough the screening of the electrons around the target nucleus affect the cross sections [9]. The ion does not fully interact with the whole charge of the target nucleus and the cross section is smaller than Rutherford cross section.

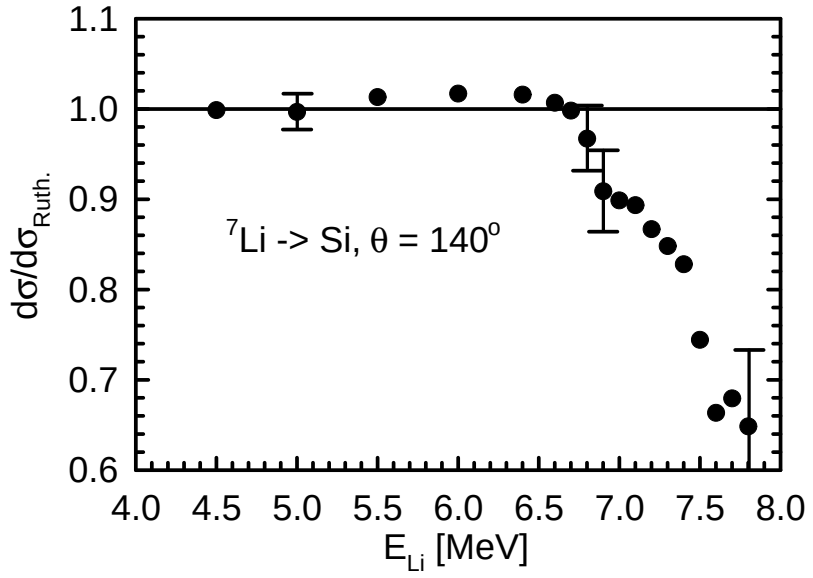

Figure 2: The ratios of the scattering cross sections to Rutherford cross sections in the shape elastic scattering for reaction Si(^{7}Li,^{7}Li)Si (data from article **IV**) as a function of energy through scattering angle of 140°. Error bars are due to statistical errors.

The screening effect decrease the cross section only some ten percents while the ion scattering from the target nucleus and the resonances may increase or decrease the scattering cross sections even by several magnitudes.

3.2.3 Shape-elastic scattering

In shape-elastic scattering the excitation curve for the ratio of the cross section to Rutherford cross section as a function of energy decreases smoothly above the non-Rutherford threshold energy. This is a result of destructive interference between the partial scattering amplitudes from Coulomb and attractive nuclear potentials. A typical excitation curve of the ratio of the cross section to Rutherford cross section for shape-elastic scattering from article **IV** is shown in Fig. 2. The reaction is Si(^{7}Li,^{7}Li)Si and the excitation curve is given as a function of energy through the scattering angle

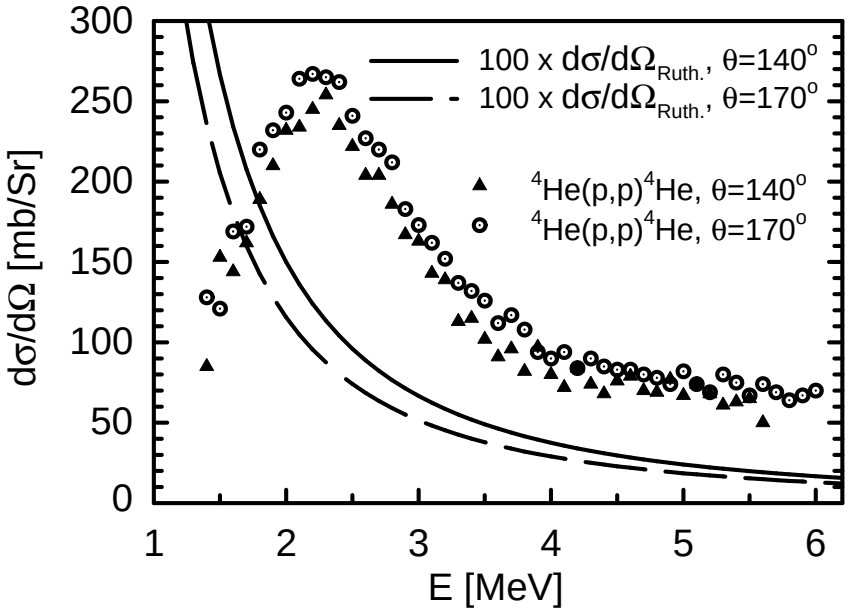

Figure 3: Resonance scattering for ^{4}He(p,p)^{4}He through the scattering angles of 140° and 170°(data from article **II**). Also the Rutherford cross sections multiplied by 100 are presented at the same scattering angles.

of 140°. At lower ion energies the $d\sigma/d\sigma_{Ruth.}$ values are near unity and after the non-Rutherford threshold energy of 6.8 MeV the excitation curve decreases smoothly and rapidly without resonance behavior, as can be seen from the figure. This behavior is typical of $d\sigma/d\sigma_{Ruth.}$ excitation curves for heavy ions and heavy targets.

3.2.4 Compound elastic scattering

Compound-elastic scattering indicates the formation of excited states in the compound nucleus created by ion and target, followed by re-emission into the elastic scattering channel. In in articles **I** and **IV** of this thesis the compound elastic scattering has been observed. Broad resonances in the cross section excitation curve refer to compound elastic scattering.

3.2.5 Resonances and resonance scattering

In all articles in this thesis resonances or resonance like behavior is observed. In articles **II** and **III** the resonance scattering with very broad and strong resonances is characteristic. The reaction investigated in these p + ^{4}He articles is

$$^1H + ^4He \rightarrow ^5Li^* \rightarrow ^1H + ^4He. \quad (6)$$

where an excited state of the compound nucleus gives rise to resonance scattering [11]. Fig. 3. illustrates the strong and broad resonance for ^{4}He(p,p)^{4}He scattering at the proton energy of about 2.2 MeV through the scattering angles of 140° and 170°. The Rutherford cross sections, which are multiplied by 100, are also shown at the same scattering angles. As can be seen from Fig. 3. the $d\sigma/d\sigma_{Ruth.}$ results range from 30 to 500 in the energy region studied. Similar results have been obtained at Sandia National Laboratories for the reaction p(^{4}He, p)^{4}He through the recoil angle of 30° in the energy range of 10 to 12 MeV [24].

Resonance scattering is more common for proton scattering by light target elements in typical energy range for materials analysis than for heavy ion scattering by heavier target elements. For example, proton scattering by carbon, nitrogen and silicon in Ref. [12], by carbon, oxygen and silicon in Ref. [13] and by beryllium in Ref. [14] have been studied and very strong resonances, where the highest $d\sigma/d\sigma_{Ruth.}$ values from 2.3 to 80 are observed in these proton-light target experiments.

3.2.6 Threshold energy for non-Rutherford cross sections

The threshold energy, where the Rutherford cross section becomes invalid, is defined as the energy where the elastic scattering cross section deviation from the Rutherford value becomes significant. In this thesis the non-Rutherford threshold energy is adopted as the energy where the measured cross

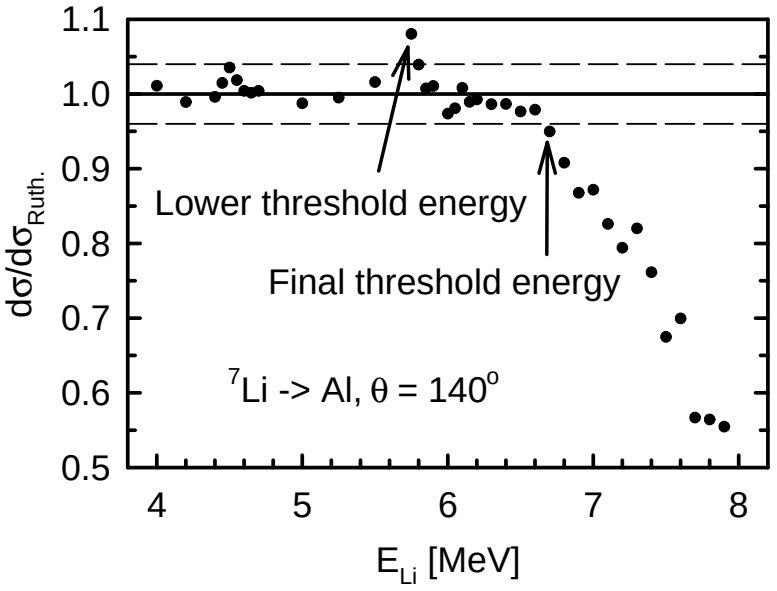

Figure 4: The lower and final threshold energy values for Al(^{7}Li,^{7}Li)Al scattering (data from article **IV**)

section values deviate 4% from the Rutherford value. In some cases there are also determined the lower threshold energy. This is due to resonance structure in a ratio of the scattering cross section to Rutherford cross section excitation curve after which the value of the ratio returns back close to unity. With higher energies than the final threshold the ratio does not reach unity. Fig. 4 illustrates the ratio of the scattering cross section to Rutherford cross section excitation curve Al(^{7}Li,^{7}Li)Al as a function of energy through the scattering angle of 140° (data from article **IV**). At the ^{7}Li ion energy of 5.75 MeV the lower and at 6.7 MeV the final threshold energies are shown by arrows. The thinner dashed lines show the 4% deviation from unity.

Some models to predict the non-Rutherford threshold energy have been developed. The classical analytical model by Bozoian et al. is based on solving the problem of Coulomb backscattering in the presence of a weak Yukawa-like nuclear potential perturbation [15–17]. They have also made a linear fit to the classical analytical calculations. According to these fits the non-Rutherford threshold energy

in the center of mass coordinates is Z_2/10 MeV for protons and Z_1Z_2/8 MeV for helium and heavier ions. Z_1 and Z_2 are the atomic numbers of the ion and target elements, respectively.

Hubbard et al. have studied also the $E_{th} = Z_1Z_2e^2/r_0(A_1^{1/3} + A_2^{1/3})^{-1}$ model, where r_0 = 1.3 fm, at the scattering angle of 180°, but noticed it to overestimate the threshold energy [18].

Also for heavier ions a model for deducing the threshold energies has been developed. Räisänen et al. have developed a $(A_1^{1/3}+A_2^{1/3})^{-1}$ dependent model. They measured the elastic scattering cross sections for carbon, nitrogen and oxygen ions by a sulfur target and made a wide literature search for other cross section data of different ion and target pairs. Then fitting the parameters to the experimental and literature data they found parameters that agreed well with their threshold energy model [21, 22].

In article **I** a threshold energy fit for protons has been presented. The second order curve was fitted to the obtained experimental threshold energies determined from the measured cross sections in the article and to the published data found by a literature survey.

These threshold energy models are dependent on the masses of the ion and the target atom, i.e., with heavier isotope of the ion one should have higher threshold energy. However, the heavier ion isotope does not automatically predict the higher experimental threshold energy when scattering by the same element. In article **IV** the determined threshold energies of ^{6}Li and ^{7}Li ion scattering by the same element are quite near to each other, but in some cases ^{6}Li has higher threshold energy than ^{7}Li in the scattering by the same element.

4 EXPERIMENTAL METHODS

All the elastic scattering cross section measurements were done at the Accelerator Laboratory of the University of Helsinki using the 2.5 MV Van de Graaff and 5 MV EGP-10-II Tandem Van de Graaff accelerators. Proton beams at energies from 1.4 to 2.7 MeV in articles **II** and **III** were obtained

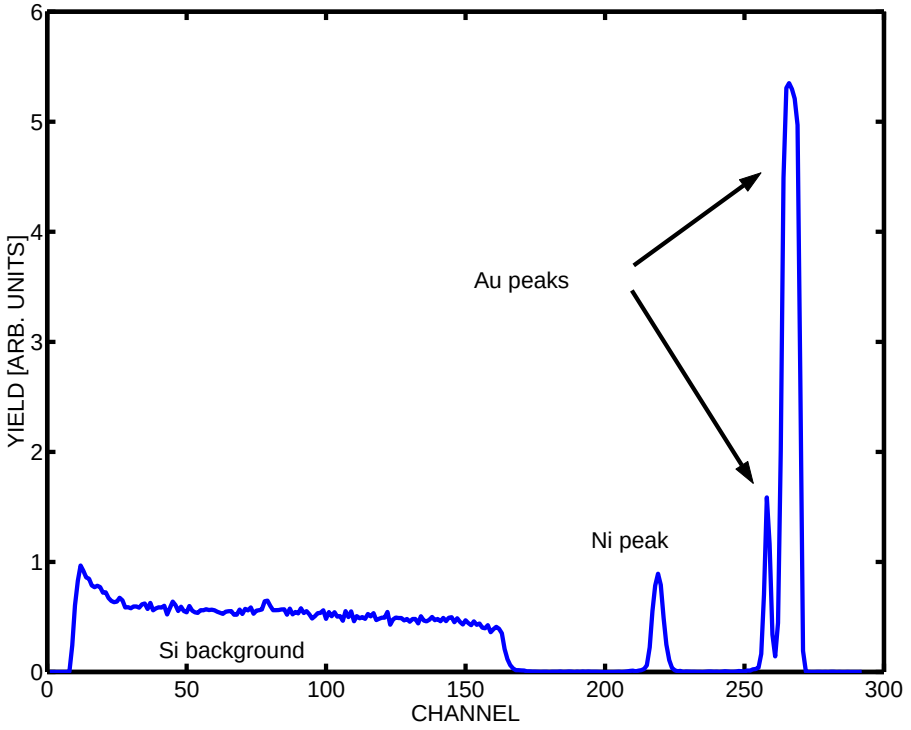

Figure 5: Measured Ni(^{4}He,^{4}He)Ni spectrum at He ion energies of 4.0 MeV through scattering angle of 137° (data from article **VI**).

from the 2.5 MV Van de Graaff accelerator. The structure of the samples, i.e., the thicknesses and the composition of the layers in articles **I**, **IV**, **V** and **VI** were determined by $^4He^+$ beam which was obtained from the Van de Graaff accelerator. All other ion beams reported in the articles were generated by the EGP-10-II accelerator.

4.1 Determination of the scattering cross sections

A typical spectrum in article **VI** for the cross section measurements is shown in Fig. 5. In the spectrum three peaks may be observed of which two originate from two thin gold films and one peak from a nickel film. The yield from the silicon wafer, on which the gold and nickel films were evaporated, may also be noticed in the spectrum. The yield of the peak in the measured spectrum depends on the elastic scattering cross section $d\sigma(E,\theta)/d\Omega$, the beam dose Q, solid angle Ω, surface density (Nt) and scattering angle θ as follows [10]:

$$A = \frac{\frac{d\sigma(E,\theta)}{d\Omega} Q\Omega(Nt)}{\cos(\theta/2)}. \quad (7)$$

Once the ratio of the yields in two peaks is obtained, the cross section may be calculated from the following formula:

$$\frac{\sigma_1(E_1,\theta)}{d\Omega} = \frac{(Nt)_2}{(Nt)_1}\frac{A_1}{A_2}\frac{d\sigma_2(E_2,\theta)}{d\Omega}, \quad (8)$$

where the subscripts 1 and 2 refer to the sample element and the reference element, respectively. The scattering cross section of the reference element is assumed pure Rutherford and Eq. (5) has been applied. Also the ratio of the cross section to Rutherford cross section of the sample element may be calculated from Eq. (8) by dividing both sides of the equation with the Rutherford cross section of the sample element.

The background subtraction procedure of the spectrum under the studied peak was done either by fitting n'th grade (n=1, 2, 3, ...) polynomial to the background or by measuring the substrate spectrum. Then by subtracting the yield under the peak the signals from the original element were counted. In some cases when very low background and extra peaks from nuclear reactions were observed in the spectrum the pure substrate spectrum was measured to distinguish the additional peaks.

The surface density (Nt) of implanted helium in tantalum foils in articles **II** and **III** was studied by the transmission-ERD measurement method. In this measurement 10.8 MeV ^{28}Si ions were used as probing beam. In Fig. (6) the simultaneously measured transmission-ERD spectrum of He(Si,He)Si recoil scattering and normal RBS spectrum of Ta(^{28}Si,^{28}Si)Ta scattering are shown.

The height of the tantalum plateau in the Ta(^{28}Si,^{28}Si)Ta backscattering spectrum is proportional to the number of Si ions collided into the foil according to Eq. (9):

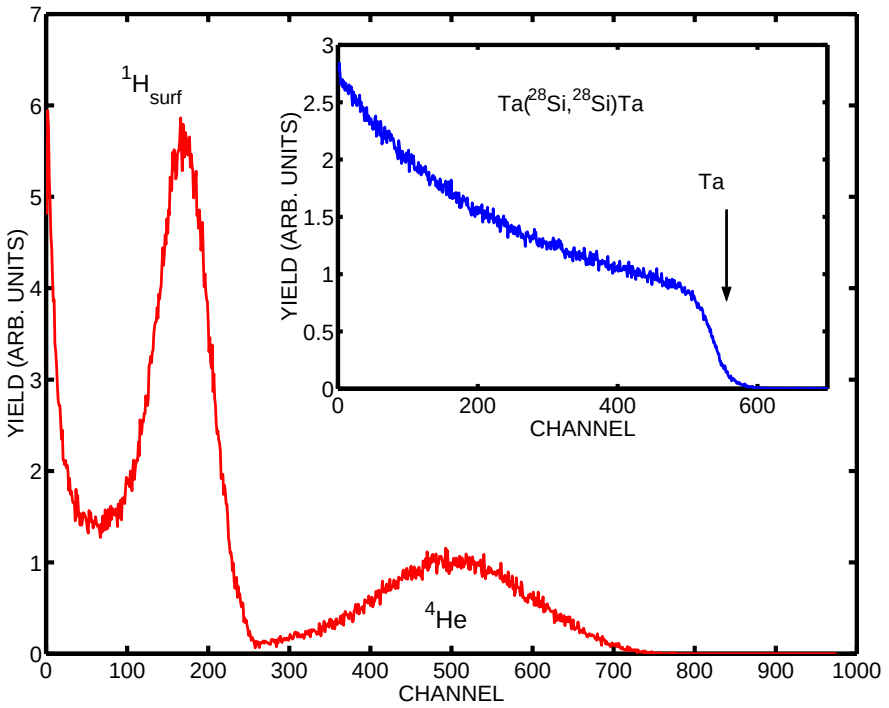

Figure 6: A ^{4}He(^{28}Si,^{4}He)^{28}Si transmission-ERD spectrum. The recoil angle was 10° and ^{28}Si ion energy 10.8 MeV. The insert shows the simultaneously measured Ta(^{28}Si,^{28}Si)Ta spectrum through the backscattering angle of 170° (data from article **II**).

$$H = \frac{d\sigma/d\Omega_{BS}\Omega_{BS}Q\delta E_{BS}}{[\varepsilon_0]\cos\theta}, \tag{9}$$

where $d\sigma/d\Omega_{BS}$ is the backscattering cross section, Ω_{BS} is the backscattering solid angle, Q is the number of incident ions, δE_{BS} is the energy/channel ratio, $[\varepsilon_0]$ is the stopping cross section factor and θ is the backscattering angle. The height (H) was determined with the GISA computer code [19]. The silicon stopping cross sections for tantalum were taken from Ref. [20], but will be determined experimentally.

The area of the helium signals in the He(Si,He)Si recoil spectrum depends on the amount of the Si ions as follows:

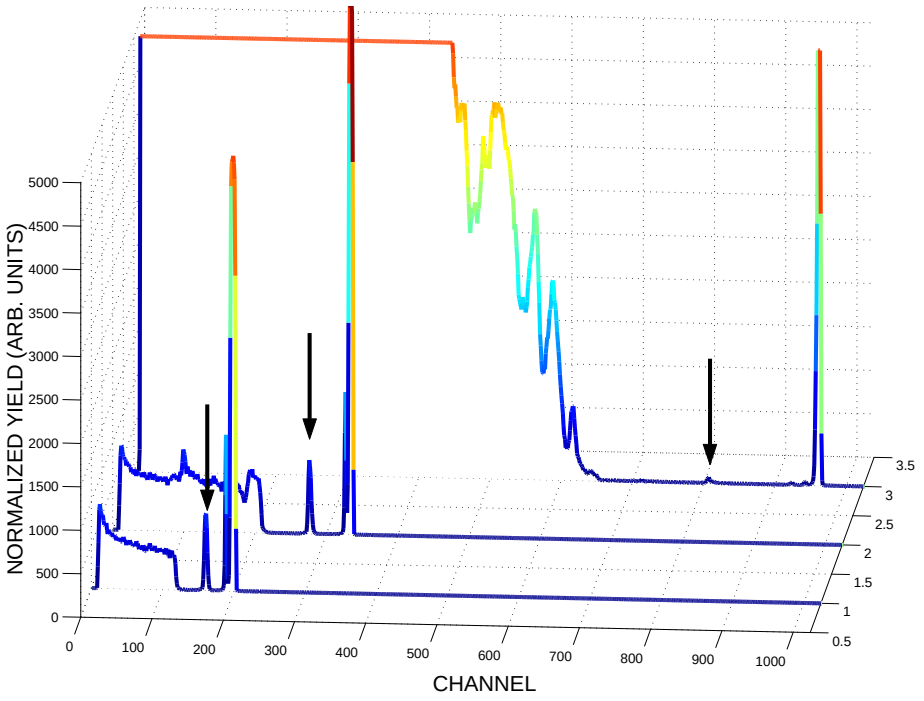

Figure 7: Measured Ni(^{4}He,^{4}He)Ni spectra at ^{4}He ion energies of 3.0, 5.0 and 14.3 MeV through scattering angle of 137° (data from article **VI**). Ni peaks are pointed by arrows.

$$A = \frac{Qd\sigma/d\Omega_{ERD}\Omega_{ERD}(Nt)}{\cos\varphi} \tag{10}$$

where Q is the number of incident ions, $d\sigma/d\Omega_{ERD}$ is the recoil scattering cross section, Ω_{ERD} is the solid angle for recoil ions, $(Nt)_{He}$ is the surface density and φ is the recoil angle.

With these equations the surface density may be determined as the number of ions is the same for both recoil and backscattering spectra. The equation for the surface density is:

$$(Nt)_{He} = \frac{Ad\sigma/d\Omega_{BS}\Omega_{BS}\delta E_{BS}}{H[\varepsilon_0]\Omega_{ERD}d\sigma/d\Omega_{ERD}}. \tag{11}$$

Fig. (7) illustrates the typical decreasing behavior of the nickel peak with increasing energy in the measurements. The three Ni(^{4}He,^{4}He)Ni spectra at energies of 3.0, 5.0 and 14.3 MeV were measured

through the scattering angle of 137°. The Ni peaks are normalized by the area of the two gold peaks in the spectra. In the first and second spectrum the nickel peak is distinguishable and in the third spectrum it can be hardly noticed.

4.2 The optical model in scattering analysis

In articles **V** and **VI** the optical model (OM) has been one of the methods by which the elastic scattering cross section results have been studied. The OM is a powerful tool for the scattering analysis because with it the cross sections at non-Rutherford energies may be predicted [7]. In the OM calculations the nuclear potential consists of two parts, real and complex one. The most commonly used OM potential is Woods-Saxon:

$$U(r) = -V_0 \frac{1}{1+e^{\frac{r-R}{a}}} - iW_0 \frac{1}{1+e^{\frac{r-R_W}{A_W}}}, \tag{12}$$

where R is the radius of the nucleus, a is the surface diffuseness which affects to the form of the nuclear potential well. Parameters R_W and A_W are the corresponding quantities for the imaginary potential.

The goal is to find the optical model parameters. It is done by solving the radial Schrödinger equation with different OM parameters and by comparing the OM cross sections with experimental data. The best fit parameters are found by using the χ-test. With the best fit parameters the cross sections may be extrapolated between data points of the studied energy and angular region.

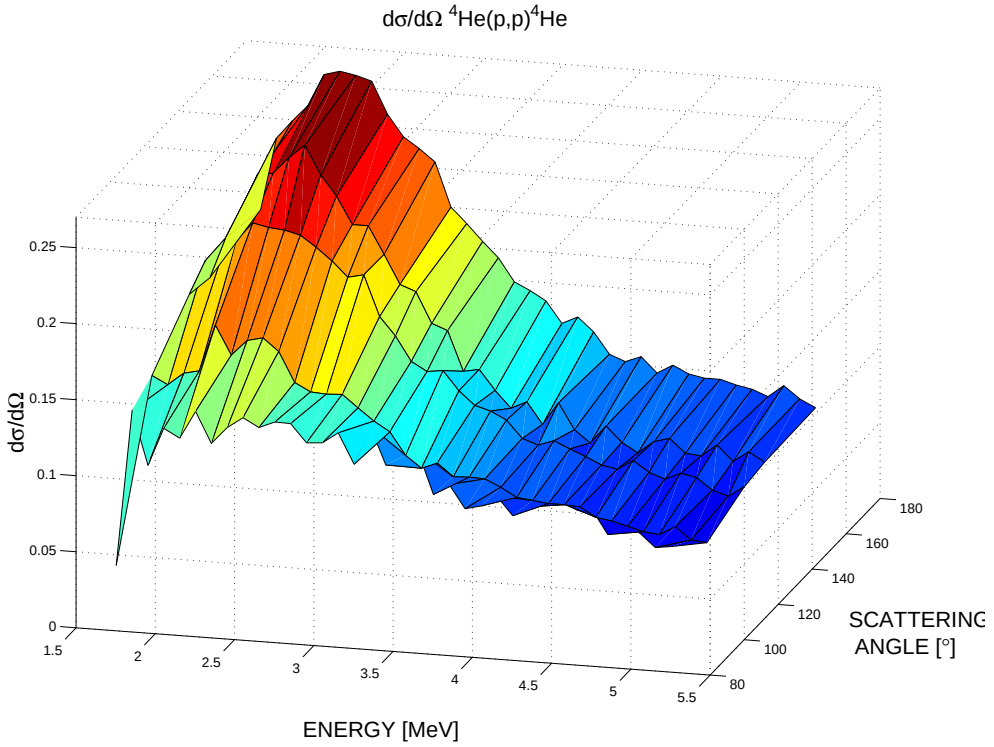

Figure 8: Elastic scattering cross sections for ^{4}He(p,p)^{4}He scattering as a function of ion energy and scattering angle (data from articles **II** and **III** and from Ref. [23]).

5 SUMMARY OF RESULTS

5.1 Proton scattering

With protons as the probing beam the ratio of cross section to Rutherford cross section excitation curve is not usually smooth. In article **I** are shown the $d\sigma/d\sigma_{Ruth.}$ curves for proton scattering by copper, molybdenum, silver and tin. For every proton-target pair the resonances are observed. For proton scattering by copper, molybdenum and tin the resonance-like behavior is more characteristic through scattering angle of 135°. The ratio of the cross section to Rutherford cross section excitation curves for protons by these elements through the scattering angle of 165° are smoother than through 135°. The threshold energies for proton scattering by silver and tin through larger scattering angles are higher. It is characteristic that the ion scattering through a larger scattering angle has lower threshold energy than trough a smaller scattering angle.

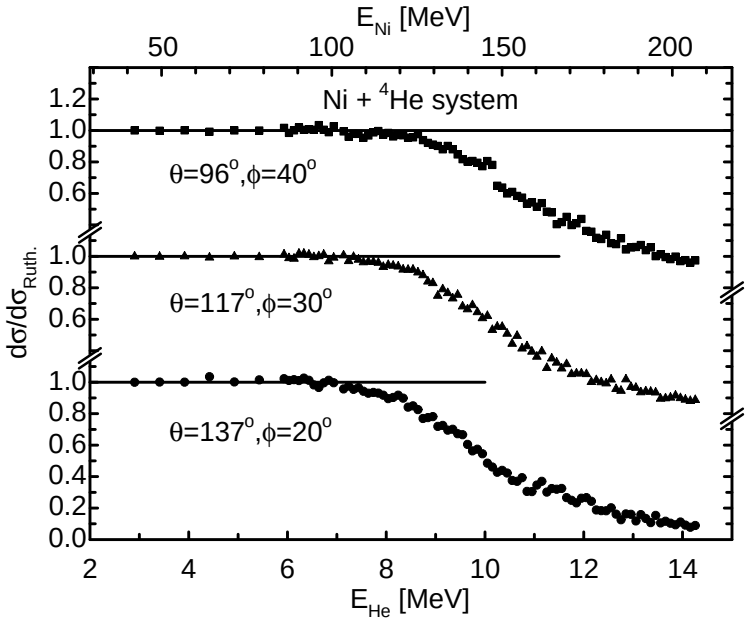

Figure 9: Measured Ni(^{4}He,^{4}He)Ni ratios of the cross section to Rutherford cross section through scattering angles θ of 96°, 117° and 137° and recoil angles φ of 40°, 30° and 20° (data from article **VI**).

Elastic scattering cross sections for ^{4}He(p,p)^{4}He scattering through the scattering angles of 85°, 106°, 128°, 140°, 170° are shown in Fig. (8). Some of the data are from articles **II** and **III** and some are from Ref. [23]. As can be seen from Fig. (8) the cross section values increase as a function of increasing backscattering angle and the local cross section maximum for all angles is at about 2.2 MeV. The ratio of the cross section to Rutherford cross section through these scattering angles range from 5 to 540. The overall trend in the angular distribution is that the proton scattering through the angle of 85° gives the minimum cross section values at almost all proton energies. Our results have been compared with recoil scattering data measured at Sandia National Laboratory by Jim Browning et al.[24] and are in excellent agreement with our data.

5.2 Helium ion scattering

In Fig. (9) the ratio of the cross section to Rutherford cross section ($d\sigma/d\sigma_{Ruth.}$) excitation curves are shown for Ni(^{4}He,^{4}He)Ni scattering as a function of energy through the scattering angles of 96°, 117° and 137° and recoil angles of 40°, 30° and 20°. All $d\sigma/d\sigma_{Ruth.}$ curves are smooth and no resonance-like behavior is observed. Therefore the scattering is shape-elastic for all measured scattering angles. We have also measured the angular distribution of scattering cross sections for the reaction Ni(^{4}He,^{4}He)Ni at the energy of 14.0 MeV. With these data we have fitted the optical model parameters and the extrapolated cross sections between the measured scattering angles (see article **VI**).

5.3 Lithium and boron ions

In articles **IV** and **V** the lithium and boron ion backscattering by several target elements is discussed. Typically the scattering of these ions near the Coulomb barrier is shape-elastic scattering and the ratio of the elastic scattering cross section to Rutherford cross section excitation curve is very smooth. Anyway, in the articles **IV** and **V** all ion-target pairs have resonance-like structure at one or more scattering angles used in the measurements.

The uncertainties in all the measured cross section values are partly due to statistical errors and uncertainties in the background subtraction. The other possible error sources are uncertainties in surface densities of the samples and solid angles. The error contribution of the surface densities are reduced by normalizing the $d\sigma/d\sigma_{Ruth.}$ values to unity at low energies in articles **I**, **IV**, **V** and **VI**.

5.4 Model for the non-Rutherford threshold energy

One of the aims in this thesis is to present a new model to predict the non-Rutherford threshold energies for helium and heavier ions through backscattering angles. Previous models, which are

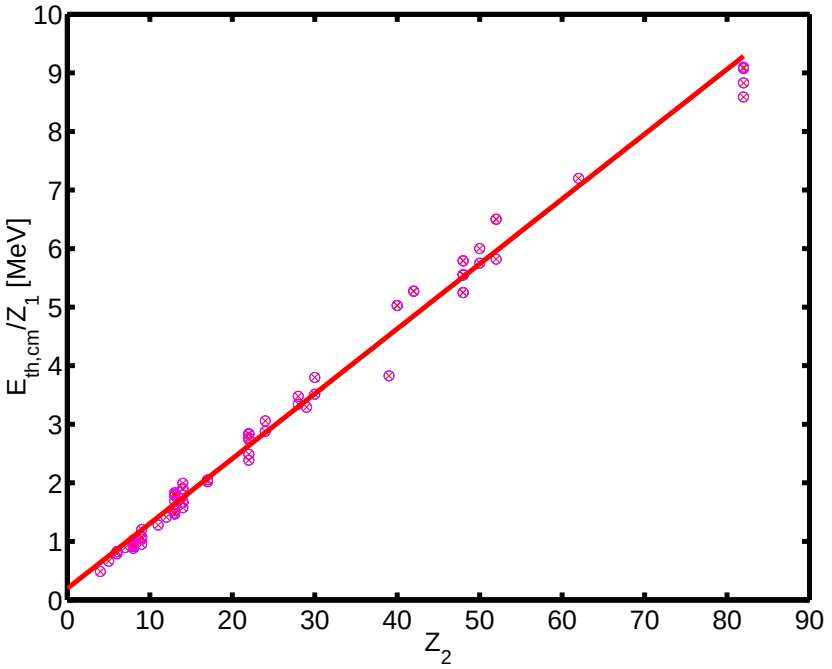

Figure 10: Previously measured and present threshold energy data as a function of target atomic number for helium and heavier ions. The threshold energies are given in the center of mass coordinates and have been divided by the ion atomic number.

discussed earlier in this thesis, are made for lighter target elements, where $Z_2 \leq 25$ and usually for protons and helium ions. Some of the models are very complicated to use and very accurate. These older models for the threshold energy are presented in Ref. [10].

We have fitted a second order equation for the proton threshold energies by heavier target elements, where $25 \geq Z_2 \geq 50$:

$$E_{th} = 7.71 \times 10^{-4} Z_2^2 + 8.12 \times 10^{-2} MeV. \quad (13)$$

The accuracy of this fit is quite good even in some cases the threshold energy is 30% below the measured value.

For heavier ions we have developed a linear fit for the non-Rutherford threshold energy. The new

elastic scattering cross section data which are measured after 1993 have been extended with the results from the older cross section measurements. The threshold model is fitted to the cross section data which are measured at scattering angles of $\theta \geq 150^{\circ}$. The ions with $2 \leq Z_1 \leq 8$ were investigated. The model estimates the threshold energy in the center of mass coordinates. When the threshold energy is given in the center of mass coordinates, the transformations to determine the laboratory energy both for recoil and backscattering processes are presented in Chapter 3.1.

The threshold energy values needed for developing the present model were extracted both from printed figures and tables given in published articles. In the procedure the energy where 4% deviation in the cross section from its Rutherford value were evaluated. The threshold energy values were usually obtained in the laboratory frame of reference and therefore the energy values were changed into the center of mass coordinates. To get a more universal fit the center of mass threshold energies were divided by the atomic number of the ion. By fitting a first order equation we obtained the following formula for the threshold energy:

$$E_{th} = \frac{Z_1 Z_2}{9} + 0.2, \tag{14}$$

where E_{th} is given in MeV and Z_1 and Z_2 are the atomic numbers of the ion and target, respectively. In Fig.10 the threshold energies are shown in the center of mass coordinates divided by the atomic number of the target. The accuracy of this model is good. The largest deviation in energy from the existing data is 0.7 MeV for Pb(^{16}O,^{16}O)Pb scattering. The largest relative deviation is 25% for Be(^{4}He,^{4}He)Be scattering. The mean deviation of the fit is less than 2%. Data from Refs. [18, 25–43] were used in model development.

As no proton data were used in developing the fit given Eq. (14), the Eq. (14) deviates from the fit presented in article **I** (Eq. (13)) by 50% at low Z_2 values, is in good agreement at Z_2 values near 45 and deviates again by 30% at Z_2 = 90.

In Table 1 the experimentally determined threshold energies presented in this thesis are summarized. The values from the measurements of article **IV** deviate 1.8%, 3.0% and 7.2% from the values predicted by the present model in Si(^{6}Li,^{6}Li)Si, Al(^{6}Li,^{6}Li)Al and Ti(^{6}Li,^{6}Li)Ti reactions, respectively.

Table 1: The non-Rutherford threshold energies (in MeV). The criterion for the threshold is defined as the energy where the cross section deviates by 4% from Rutherford cross section. The laboratory scattering angles are indicated. Superscript 1 indicates a threshold energy taken from a resonance.

Ion	Target	Threshold energies			
		$\theta = 135^\circ$	$\theta = 165^\circ$	Analytical model (Refs. [15–17])	
Proton	Cu	3.5	3.4	2.8	
	Mo	5.1	5.0	4.0	
	Ag	5.0	5.8	4.5	
	Sn	6.1	6.2	4.7	
		$\theta = 96^\circ$	$\theta = 117^\circ$	$\theta = 137^\circ$	
^{4}He	Ni	7.54^1	7.84	7.14^1	
		8.44^1		7.34^1	
		8.74		7.54	
				Analytical model	Simplified formula $\frac{Z_1 Z_2}{8}\frac{(m_1+m_2)}{m_1}$
		$\theta = 140^\circ$	$\theta = 170^\circ$	(Refs. [15–17])	
^{6}Li	Al	6.15^1	6.20	5.44	5.96
		6.40			
	Si	6.60^1	6.25^1	5.87	6.37
		6.70	6.50		
	Ti	8.90^1	8.85^1	8.35	9.28
		9.25	9.55		
^{7}Li	Al	5.75^1			
		6.65			
	Si	6.80			
	Ti	8.40^1			
		8.95			
		$\theta = 115^\circ$	$\theta = 135^\circ$		
	Ni	10.4^1	11.7^1		
		11.7	12.4		
		$\theta = 89^\circ$	$\theta = 110^\circ$	$\theta = 132^\circ$	
^{11}B	Ni	19.0^1	18.0^1	21.4	
			22.5		

6 CONCLUSIONS

In this thesis the elastic scattering cross sections of several ions by many target elements have been investigated as well as the non-Rutherford threshold energies have been determined. A simple but still quite accurate model to predict the threshold energy for the non-Rutherford scattering has been presented.

Elemental analysis and depth profiling with proton backscattering in ion beam analysis becomes more difficult when nuclear reactions arise. If the non-Rutherford energy region is applied in the measurements the analysis of the measured spectrum should be done with advanced computer programs like GISA [19] or IBA DataFurnace [44–48]. Typical impurities on sample surfaces, like hydrogen, carbon and oxygen, may cause unexpected effects to the measured backscattering spectrum. In proton scattering, resonances are characteristic in the cross section excitation curve. Even with heavier target elements like molybdenum and tin, a resonance-like structure are observed in the cross section excitation curve. Because of smaller nuclear contributions, heavier ions may be more suitable even for lighter target elements when higher energy ion beams are applied. If the measurements are to be done in the Rutherford scattering energy region, the energy limit is defined usually by the lightest target element. For example, with protons as probing beams the energy region in the measurements is quite limited.

One of the future prospects is to determine the full energy and angular windows for the Rutherford backscattering spectrometry. By measuring the effects of electronic screening to the cross sections the threshold for Rutherford scattering in 4% accuracy at low energies and small scattering angles may be determined.

The work with the hydrogen standard is still unfinished. The co-operation with Sandia National Laboratory to make the standard has been fruitfully started and will be continued. The task in the

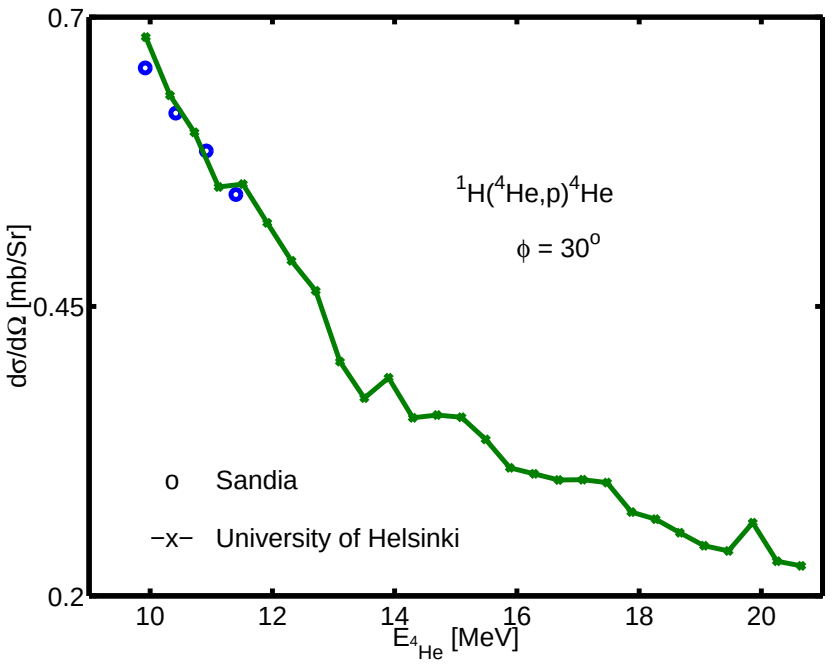

Figure 11: The recoil cross sections for the $^{1}H(^{4}He,p)^{4}He$ scattering through the recoil angle of 30°. The circles are the values by the Sandia group and the crosses are the kinematically reversed cross sections by the Helsinki group. The solid line has been drawn to guide the eye.

project will be high accuracy elastic scattering cross section measurements for the $^{1}H(^{4}He,p)^{4}He$ reaction.

In the hydrogen standard project we have so far measured $^{4}He(p,p)^{4}He$ cross sections through the scattering angles of 85°, 106° and 128° in the energy range from 1.2 to 5.2 MeV. When the scattering of $^{4}He(p,p)^{4}He$ reaction is reversed kinematically to $^{1}H(^{4}He,p)^{4}He$ reaction the recoil angles are 40°, 30° and 20°, respectively. The energy range for the reversed reaction is from 4.8 to 20.6 MeV. The Sandia group has made recoil cross section measurements for the reaction $^{1}H(^{4}He,p)^{4}He$ [24]. They have measured the cross sections through the recoil angle of 30° in the energy range from 9.9 to 11.7 MeV. Fig. (11) shows the recoil cross section results of the Sandia measurements and our kinematically reversed cross sections through the recoil angle of 30°. The circles illustrate the Sandia measurements and the crosses are our kinematically reversed cross sections. The solid line has been drawn to guide the eye. The figure shows that the deviation between the four cross section data points obtained at Sandia and our data is negligible.

ACKNOWLEDGEMENTS

This study was carried out in the Accelerator Laboratory between the years 1996 and 2001. I wish to thank Prof. Juhani Keinonen for giving me the opportunity to work at the Accelerator Laboratory and placing the facilities of the Laboratory at my disposal. I am indebted to my advisors Prof. Jyrki Räisänen and Doc. Eero Rauhala, the former and present heads of the Accelerator Laboratory for their excellent guidance and never ending patience in teaching me the experimental physics.

I thank my co-worker Petteri Pusa, M.Sc., for fruitful and most efficient working atmosphere, interesting and stimulating conversations and ways of seeing things in the Laboratory and elsewhere. I also thank my other co-authors who have collaborated in these articles. Warm thanks go to all my co-workers who have created a pleasant atmosphere for working in the Lab.

I thank the technical staff, especially Mr. Raimo Ingren, Mr. Heikki Sepponen and Lab. Eng. Kim Wahlström for operation of the accelerators. I am indebted to Mr. Mauri Kurki, Mr. Sakari Sariola and Mr. Pasi Siiki for preparing the equipment and to Mr. Jari Urkio for making samples for the measurements.

My warmest thanks go to my son, Jeremias, who has been the light of my life. I also thank all the other people who have closely followed this process for their support and encouragement.

Financial support from the Magnus Ehnrooth foundation, the Armas Kordelin foundation, the Finnish Physical Society and the Academy of Finland is gratefully acknowledged.

Helsinki, March 2001

Arto Nurmela

REFERENCES

1. H. Geiger and E. Marsden, *Phil. Mag.* **25** (1913) 606.
2. E. Rutherford, *Phil. Mag.* **21** (1911) 669.
3. S. Rubin and V.K. Rasmussen, *Phys. Rev.* **78** (1950) 83.
4. R.F. Sippel, *Phys. Rev.* **115** (1959) 1441.
5. A.L. Turkevich et al., in Surveyor Final Report, Part II, Scientific Results, Nat. Aeronaut. and Space Administration Tech. Rep. 32-1265, pp. 303-387, Jet Propulsion Lab., California Inst. if Technol., Pasadena, California.
6. W.K. Chu, J.W. Mayer and M.A. Nicolet, Backscattering Spectrometry, Academic Press, London, 1978.
7. P.E. Hodgson, The Optical Model of Elastic Scattering, Oxford University Press, London 1963.
8. S. Gasiorowicz, Quantum Physics, John Wiley and Sons, New York, 1974.
9. R.D. Evans, The Atomic Nucleus, Mc Graw-Hill, New York, 1965.
10. J.R. Tesmer and M. Nastasi (eds.), Handbook of Modern Ion Beam Materials Analysis, Materials Research Society, Pittsburgh, 1995.
11. G. Freier, E. Lampi, W. Sleator and J.H. Williams, *Phys.Rev.* **75** (1949) 1345.
12. E. Rauhala, *Nucl. Instr. and Meth.* **B 12** (1985) 447.
13. R. Amirikas, D.N. Jamieson, S.P. Dooley, *Nucl. Instr. and Meth.* **B 77** (1993) 110.
14. Zheming Liu and Ron Wang, *Nucl. Instr. and Meth.* **B 93** (1994) 404.
15. M. Bozoian, K.M. Hubbard and M. Nastasi, *Nucl. Instr. and Meth.* **B 51** (1990) 311.
16. M. Bozoian, *Nucl. Instr. and Meth.* **B 56/57** (1991) 740.
17. M. Bozoian, *Nucl. Instr. and Meth.* **B 82** (1993) 602.
18. K.M. Hubbard, J.R. Tesmer, M. Nastasi and M. Bozoian, *Nucl. Instr. and Meth.* **B 58** (1991) 121.
19. J. Saarilahti and E. Rauhala, *Nucl. Instr. and Meth.* **B 64** (1992) 734.
20. J. Ziegler, SRIM-96 computer code, private communication.
21. J. Räisänen, E. Rauhala, J.M. Knox and J.F. Harmon, *J. Appl. Phys.* **75** (1994) 3273.
22. J. Räisänen and E. Rauhala, *J. Appl. Phys.* **77** (1995) 1762.
23. Proceedings of HDT Workshop, Sandia National Laboratories, April 13-14, 2000, private communication.

24. J.F. Browning, R.A. Langley, B.L. Doyle, J.C. Banks and W.R. Wampler, *Nucl. Instr. and Meth.* **B 161-163** (2000) 211.

25. Z.S. Zheng, J.R. Liu, X.T. Cui and W.K. Chu, *Nucl. Instr. and Meth.* **B 118** (1996) 214.

26. J.A. Leavitt, P. Stoss, D.B. Cooper, J.L. Seerveld, L.C. McIntyre Jr, R.E. Davis, S. Gutierrez and T.M. Reith, *Nucl. Instr. and Meth.* **B 15** (1986) 296.

27. J.A. Leavitt, L.C. McIntyre Jr, P. Stoss, J.G. Oder, M.D. Ashbaugh, B. Dezfouly-Arjomandy, Z.M. Yang and Z. Lin, *Nucl. Instr. and Meth.* **B 40-41** (1989) 776.

28. J.A. Leavitt, L.C. McIntyre Jr, R.S. Champlin, J.O. Stoner Jr, Z. Lin, M.D. Ashbaugh, R.P. Cox and J.D. Frank, *Nucl. Instr. and Meth.* **B 85** (1994) 37.

29. C. Huan-sheng, S. Hao, Y. Fujia and T. Jia-yong, *Nucl. Instr. and Meth.* **B 85** (1994) 47.

30. Y. Feng, Z. Zhou, Y. Zhou and G. Zhao, *Nucl. Instr. and Meth.* **B 86** (1994) 225.

31. C. Huan-sheng, S. Hao, Y. Fujia and T. Jiayong, *Chinese Journal of Nuclear Physics* **15** (1993) 333.

32. C. Huan-sheng, Y. Fujia, Z. Guoqing, Z. Chengteng, W. Shiming and Y. Xiaowei, *Nuclear Techniques* **13** (1990) 392.

33. Y. Eisen, E. Abramson, G. Engler, M. Samuel, U. Smilansky and Z. Vager, *Nucl. Phys.* **A 236** (1974) 327.

34. G.M. Hudson and R.H. Davis, *Phys. Rev.* **C 9** (1974) 1521.

35. I. Badawy, B. Berthier, P. Charles, M. Dost, B. Fernandez, J. Gastebois and S.M. Lee, *Phys. Rev.* **C 17** (1978) 978.

36. Z. Pastuovic, M. Jaksic, T. Tadic and P. Oliaiy, *Nucl. Instr. and Meth.* **B 136-137** (1998) 81.

37. E. Rauhala and J. Räisänen, *Nucl. Instr. and Meth.* **B 35** (1988) 7.

38. J. Räisänen and E. Rauhala, *Nucl. Instr. and Meth.* **B 73** (1993) 439.

39. E. Rauhala and J. Räisänen, *J. Appl. Phys* **75** (1994) 642.

40. D. Abriola, D. DiGregorio, J.E. Testoni, A. Etchegoyen, M.C. Etchegoyen, J.O. Fernandez-Niello, A.M.J. Ferrero, S. Gil, A.O. Macchiavelli, A.J. Pacheco and J. Kittl, *Phys. Rev.* **C 39** (1989) 546.

41. S. Salem-Vasconcelos, E.M. Takagui, N.J. Bechara, K. Koide, O. Dietzsch, A. Bairrio-Nuevo Jr and H. Takai, *Phys. Rev.* **C 50** (1994) 927.

42. Y. Eisen, R.A. Eisenstein, U. Smilansky and Z. Vager, *Nucl. Phys.* **A 195** (1972) 513.

43. J.S. Lilley, M.A. Nagarajan, D.W. Banes, B.R. Fulton and I.J. Thompson, *Nucl. Phys.* **A 463** (1987) 710.

44. N.P. Barradas, C. Jeynes, R.P. Webb, *Appl. Phys. Lett.* **71** (1997) 291.

45. N.P. Barradas, P.K. Marriott, C. Jeynes, R.P. Webb, *Nucl. Instr. and Meth.* **B 136-138** (1998) 1157.

46. N.P. Barradas, C. Jeynes, M.A. Harry, *Nucl. Instr. and Meth.* **B 136-138** (1998) 1163.

47. N.P. Barradas, C. Jeynes, S.M. Jackson, *Nucl. Instr. and Meth.* **B 136-138** (1998) 1168.

48. C. Jeynes, N.P.Barradas, and J.Wilde, *Nucl. Instr. and Meth.* **B 161-163** (2000) 287.